PAPER

Impact of CH₄ addition on the electron properties and electric field dynamics in a Ar nanosecondpulsed dielectric barrier discharge

To cite this article: Timothy Y Chen et al 2022 Plasma Sources Sci. Technol. 31 125013

View the article online for updates and enhancements.

You may also like

- Diagnostics of a nanosecond atmospheric plasma jet. Electron and ro-vibrational excitation dynamics Nikolay Britun, Peter Raj Dennis Christy,
- Vladislav Gamaleev et al.
- Characterization of an atmospheric pressure plasma jet producing the auroral transition O(\frac{1}{S}) to O(\frac{1}{D}) S Jaiswal, E M Aguirre and T van der Gaag
- Vibrational kinetics in repetitively pulsed atmospheric pressure nitrogen discharges: average-power-dependent switching behaviour

Helen L Davies, Vasco Guerra, Marjan van der Woude et al.



Impact of CH₄ addition on the electron properties and electric field dynamics in a Ar nanosecond-pulsed dielectric barrier discharge

Timothy Y Chen^{1,3,5}, Xingqian Mao^{1,5}, Hongtao Zhong¹, Ying Lin¹, Ning Liu¹, Benjamin M Goldberg^{1,4}, Yiquang Ju¹ and Egemen Kolemen^{1,2,*}

E-mail: ekolemen@princeton.edu

Received 14 June 2022, revised 9 November 2022 Accepted for publication 14 December 2022 Published 3 January 2023



Abstract

Non-equilibrium plasmas derive their low temperature reactivity from producing and driving energetic electrons and active species under large electric fields. Therefore, the impact of reactants on the plasma properties including electron number density, electric field, and electron temperature is critical for applications such as plasma methane (CH₄) reforming. Due to experimental complexity, electron properties and the electric field are rarely measured together in the same discharge. In this work, we combine time-resolved Thomson scattering and electric field induced second harmonic generation to probe electron temperature, electron density, and electric field strength in a 60 Torr CH₄/Ar nanosecond-pulsed dielectric barrier discharge while varying the CH₄ mole fraction from 0% to 8%. These measurements are compared to a 1D numerical model to benchmark its predictions and identify areas of uncertainty. Nonlinear coupling between CH₄ addition, electron temperature, electron density, and the electric field was directly observed. Contrary to previous measurements in He, the electron temperature increased with CH₄ mole fraction. This rise in electron temperature is identified as electron heating by residual electric fields that increased with larger CH₄ mole fraction. Moreover, the electron number density has been found to decrease rapidly with the increase of methane mole fraction. Comparison of these measurements with the model yielded better agreement at higher CH₄ mole fractions and with the usage of ab initio calculated Ar electron-impact cross-sections from the B-spline R-matrix database. Furthermore, the calculated plasma properties are shown to be sensitive to the residual surface charge implanted on the quartz dielectric surfaces. Without considering surface charge in the simulations, the calculated electric field profiles agreed well with the measurements, but the electron properties were underpredicted by more than a factor

¹ Department of Mechanical and Aerospace Engineering, Princeton University, Princeton, NJ 08544, United States of America

² Princeton Plasma Physics Laboratory, Princeton, NJ 08544, United States of America

³ Present address: Sandia National Laboratories, Livermore, CA, 94550.

Present address: Lawrence Livermore National Laboratories, Livermore, CA, 94550.

⁵ These authors contributed equally to this work.

Author to whom any correspondence should be addressed.

of three. Therefore, measurements of either the electric field or electron properties measurements alone are insufficient to fully validate modeling predictions.

Supplementary material for this article is available online

Keywords: Thomson scattering, electric field, plasma CH₄ reforming, electric field induced second harmonic generation, electron density, electron temperature, nanosecond-pulsed discharge

(Some figures may appear in colour only in the online journal)

1. Introduction

In recent years, atmospheric levels of methane (CH₄), a major greenhouse gas, have been rising [1], and CH₄ emissions have contributed more than 20% of the total increase in global temperatures to date [2]. Therefore, development of a method utilizing renewable electricity to process CH₄ can make a great contribution toward fighting global climate change. There is increasing interest in using electrically-driven non-equilibrium plasma discharges for CH₄ reforming and catalysis to process this potent greenhouse gas [3–5]. However, most studies rely on *ex-situ* sampling of products [3, 4, 6–8] and relatively few experiments make time-resolved *in situ* measurements of CH₄-containing non-equilibrium plasmas [9–13]. As a result, the plasma chemistry is not well-understood due to the lack of *in situ* quantification of the plasma properties and species.

In non-equilibrium plasma discharges, the plasma chemistry is initiated by electron-impact reactions with the neutral gas species. Whether the gas molecules are excited, dissociated, or ionized, depends on the electron energy distribution function. In between collisions with the neutral gas, the electrons gain energy from the applied electric field. The amount of non-equilibrium excitation and reactivity these electrons can induce in the neutral gas depends on the electron energy and the electron number density. As a result, the electron dynamics and plasma chemistry are intimately linked to the electric field and the plasma chemistry. Furthermore, the reactant composition also influences the available electron-molecule energy transfer pathways. Therefore, it is critical to quantitatively understand how both the electron properties and electric field evolve in time and change with mixture composition.

Advances over the years in time-resolved *in situ* laser diagnostics have enabled investigations of the electron number density [9, 14–20], electron temperature [9, 14–19] and electric field [21–32]. However, these studies rarely measure all of these quantities together in the same plasma and compare them against plasma kinetic modeling, especially for varying reactant compositions. Oftentimes, only a single parameter is measured and used for model validation. For example, in [22], four wave mixing was used to measure the electric field with sub-nanosecond temporal resolution and validate model predictions of the electric field in a nanosecond-pulsed dielectric barrier discharge (ns-DBD). However, experimental electron number density measurements were unavailable for model validation. Likewise, laser Thomson scattering has been used to

characterize the time-resolved electron density and temperature of a nanosecond-pulsed discharge without any measurements of the electric field [9, 17–19].

The development of electric field induced second harmonic generation (EFISH) as a plasma diagnostic [23] has sparked a recent rise of electric field measurements in the literature. Applications of this technique range from atmospheric pressure plasma jets [26] to flames [27, 28] to nanosecondpulsed discharges [25, 33, 34]. In a centrosymmetric medium, like a gas, second order nonlinear optical processes such as second harmonic generation are forbidden. However, the presence of an external electric field breaks this symmetry and allows the generation of second harmonic light through a third-order nonlinear optical process. EFISH has some distinct advantages over other electric field measurement techniques. Unlike laser-induced fluorescence dip or four wave mixing, EFISH is a nonresonant laser diagnostic [32]. This allows a single laser to be used with a wide variety of gas compositions and pressures, since it does not depend on a resonance with an atomic or a molecular gas and is not limited by pressure broadening. This also simplifies the experimental setup, since a Raman cell or a dye laser for tuning the laser wavelength is unnecessary. Furthermore, EFISH can be performed with nanosecond [29, 30], picosecond [24, 25], and femtosecond pulse-width lasers [23, 26, 34] of a variety of pump laser wavelengths, facilitating implementation across different laboratories and measurements with nanosecond to sub-nanosecond temporal resolution. Spectrallyresolved streak camera imaging of nanosecond-pulsed discharges has been demonstrated with sub-nanosecond time resolution [35]. This development suggests the possibility of sub-nanosecond electric field measurements using emission spectroscopy, but such measurements so far would be limited to gas mixtures containing certain species such as He [36] or N₂ [37]. Additionally, there are large uncertainties in the models used for determining the electric field [38, 39] and the sensitivity for Stark polarization spectroscopy is reduced at low electric field strengths ($<4 \,\mathrm{kV \, cm^{-1}}$ in [36]). Lastly, these techniques cannot provide information without any plasma emission.

Laser Thomson scattering is a well-established technique for quantifying the electron temperature and electron density simultaneously in both equilibrium and non-equilibrium plasmas [16, 40–43]. Thomson scattering results from photons scattering off of charged species, so the electron properties can be directly interpreted from the Thomson scattering spectrum.

This is in contrast to optical emission spectroscopy or laser-collision induced fluorescence which require a collisional-radiative model for extracting electron properties. Recently, there has been a growing number of laser Thomson scattering studies of nanosecond-pulsed plasmas in the literature [9, 17–19, 44], but few have focused on volumetric ns-DBDs used previously for plasma-assisted combustion and CH₄ reforming kinetics studies [13, 45–47]. Due to the complexity of the plasma chemistry in these plasma-assisted combustion and CH₄ reforming studies, detailed investigations of the plasma properties in a simpler gas mixture containing hydrocarbons would be highly desirable.

In this study, we used both EFISH and Thomson scattering to measure the time-resolved electric field, electron temperature, and electron density of CH₄/Ar ns-DBD plasmas with varying concentrations of CH₄. With these measurements, the major plasma properties were characterized and the underlying coupling between these parameters was studied. We show that addition of hydrocarbons nonlinearly altered the electron properties as well as the peak electric fields at breakdown. Furthermore, we demonstrate a direct coupling between the post-breakdown electric field, electron density, and electron temperature. The experimental measurements were compared to a numerical model to evaluate its predictions of plasma properties. From these comparisons, we identified key areas of uncertainty in the model, namely the impact of residual surface charge from previous pulses and the electron-impact cross-sections. Finally, we demonstrate that model agreement with experimentally measured electric fields does not guarantee quantitative prediction of electron properties and vice versa.

2. Experimental and numerical methods

2.1. Nanosecond-pulsed dielectric barrier discharge cell

The ns-DBD flow reactor cell previously described in [9, 34] was used in this study. The ns-DBD had a gap distance of 14 mm and 44.5 mm square electrodes. The plasma was generated by a nanosecond-pulse power supply (FID GmBH) with an amplitude of 8.5 kV and frequency of 500 Hz. The power supply had two output leads which carried either a positive and negative voltage pulse. When both output leads were connected across the ns-DBD, the overall voltage across the gap was approximately doubled compared to using either the positive or negative side alone. The voltage pulse profiles measured by a high voltage probe (P6015A, Tektronix) are plotted in figure 1. This particular nanosecond pulser generates several sub-pulses that have been measured previously by EFISH and demonstrated to represent an electric field applied to the discharge rather than electrical noise from the nanosecondpulse power supply [34]. Mass flow controllers (MKS) set the flow speed of the gas in the discharge cell to $0.3 \,\mathrm{m \, s^{-1}}$ and a downstream control valve (153D, MKS) stabilized the pressure at 60 Torr. A 99.997% pure Ar gas cylinder and a 99.5% pure CH₄ gas cylinder were used. All of the electronic timings were synchronized via a digital delay/pulse generator (DG645, Stanford Research Systems).

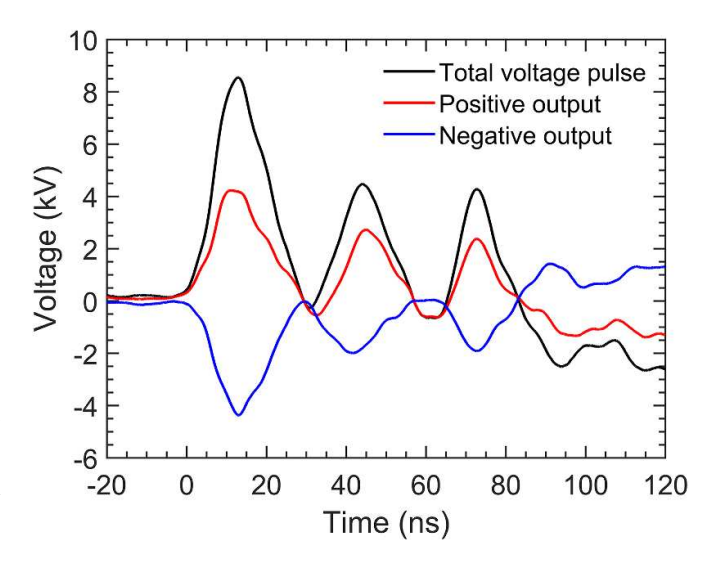


Figure 1. Measured positive, negative, and total voltage applied across the discharge gap from the nanosecond-pulse power supply.

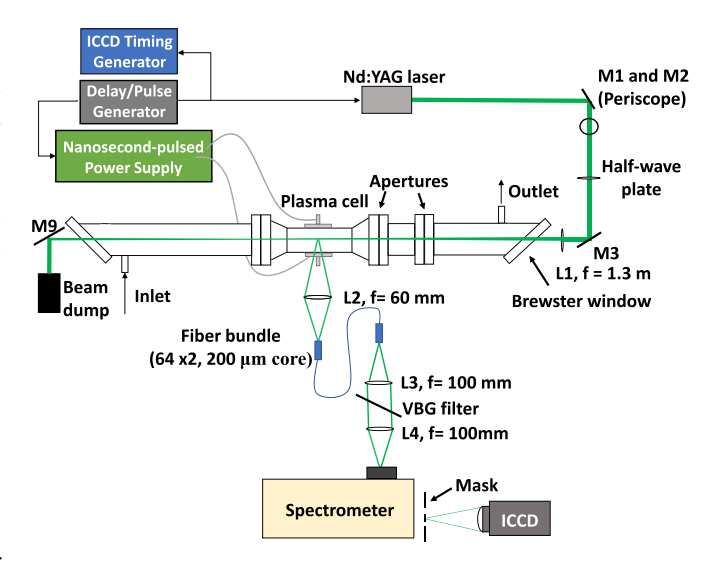


Figure 2. Experimental setup for Thomson scattering. A volume Bragg grating notch filter (VBG) was used in conjunction with a physical mask to reject stray light and Rayleigh scattering.

2.2. Thomson scattering

In this study, the Thomson scattering apparatus described in [9] was modified with the addition of a fiber bundle and OD4 volume Bragg grating notch filter (BNF-532-OD4-12.5M, Optigrate, $<7\,\mathrm{cm^{-1}}$ full-width at half maximum (FWHM)) in the collection optics. The experimental schematic is shown in figure 2. Briefly, a frequency-doubled Q-switched Nd:YAG laser (Q-smart 850, Quantel) producing 390 mJ pulses at 532 nm was focused to the middle of the ns-DBD using a 1300 mm focal length lens. An achromatic aspheric lens (Edmund Optics) was used to collect the scattered laser light and input it into a custom 64×2 fiber bundle. Each fiber had a 200 micron core diameter. The output of the fiber bundle was collimated with a $f=100\,\mathrm{mm}$ lens and a volume Bragg grating notch filter was used to reject 532 nm light. Without the

filter, Rayleigh scattering and stray light would overwhelm the weak Thomson scattering signal. Due to the narrow acceptance angle of the filter, only 6 mm of a single row of fibers had sufficient stray light rejection, and the region of interest on the camera was adjusted accordingly. The residual filtered light was then focused onto the 300 μ m wide spectrometer slit. A blackened mask (1 nm FWHM rejection linewidth) was placed at the spectrometer focal plane to completely block 532 nm light and enable on-chip accumulation on the intensified charge coupled device (ICCD) camera (PIMAX 1300, Princeton Instruments). About 200 laser shots were accumulated on-chip and 50 to 150 frames were captured per time delay. In total, 10 000 to 30 000 laser shots were averaged per data point. The error was evaluated from the 95\% confidence intervals of the fit to the Thomson scattering spectrum. Rotational Raman scattering of N₂ at 60 Torr was used for absolute calibration of the electron number density. Details regarding the fitting routine and calibration can be found in [9].

2.3. Electric field-induced second harmonic generation

The experimental schematic for EFISH is shown in figure 3. A 400 mm focal length spherical lens was used to focus 350 μ J laser pulses from a femtosecond Ti:sapphire regenerative amplifier (Astrella, Coherent) to the center of the ns-DBD. The regenerative amplifier produces 80 fs pulses centered around 800 nm at 1 kHz repetition rate with a transform limited bandwidth of approximately 12 nm. A long pass filter was placed right before the discharge cell to remove any second harmonic light generated upstream. The second harmonic signal generated was separated using both a dispersive prism as well as a dichroic mirror that reflects 400 nm and transmits 800 nm light. An ICCD in combination with a 400 nm bandpass filter (65–193, Edmund Optics) with $\pm 10 \, \text{nm}$ FWHM was used to detect the EFISH signal. At each time delay, 250 frames were captured on the ICCD (PIMAX4, Princeton Instruments) for averaging, and on-chip accumulations of four laser shots were captured per frame, resulting in 1000 individual laser shots per data point. The image intensifier can repetitively gate much faster than the CCD readout speed, so this scheme allowed faster data acquisition and improved signal-to-noise ratios. The ICCD camera gate was 60 ns which limited interference by plasma emission. A delay generator (DG645, Stanford Research Systems) was used to delay the nanosecond pulser from the femtosecond laser pulse and trigger the ICCD camera for time-resolved measurements. Timing jitter was measured on a 10 GS/s oscilloscope (Tektronix) using a 150 ps rise time photodiode (DET 025, Thorlabs) and a high voltage probe (P6015A, Tektronix) to be less than 300 ps. Therefore, the EFISH time delay scan was performed with 500 ps time steps while ensuring sub-nanosecond temporal resolution of the averaged measurements. The plasma emission was recorded for each time step and subtracted from the EFISH signal. EFISH calibration was performed via measuring sub-breakdown electric fields using an AC power supply in each of the gas mixtures studied. This allowed calibration that matched the experimental discharge geometry and gas composition as close as possible.

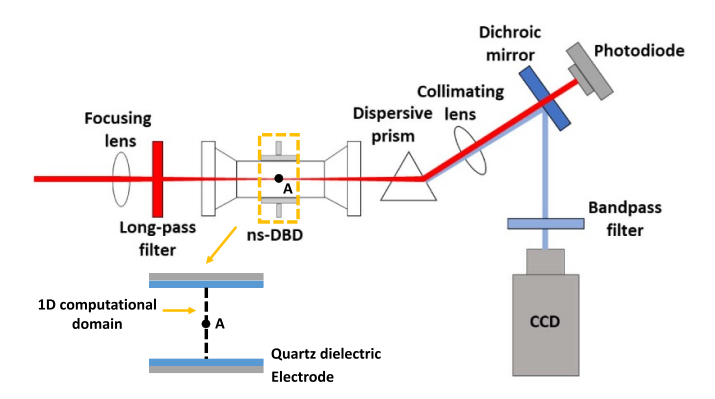


Figure 3. Experimental setup and 1D computational domain for electric field-induced second harmonic generation.

2.4. Numerical model

The numerical modeling is conducted by a multi-scale adaptive reduced chemistry solver for plasma assisted combustion (MARCS-PAC) [48, 49]. The model integrates the experimentally validated 2D plasma solver PASSKEy (PArallel Streamer Solver with KinEtics) [50-53] and the adaptive simulation of unsteady reactive 2D flow solver ASURF+ [54–56]. The drift-diffusion-reaction equations for plasma species, Helmholtz equations for photoionization, Poisson equation for electric field, energy conservation equation for electron and plasma discharge as well as unsteady, multi-component, reactive, compressible Naiver-Stokes equations are coupled by time splitting solution methods. The detailed governing equations and numerical schemes have been described in [48]. Note that the electron temperature during the discharge is obtained by the local mean energy approximation. The mean electron energy $\bar{\epsilon_e}$ is calculated by

$$\frac{\partial n_e \bar{\epsilon_e}}{\partial t} + \vec{\nabla} \cdot \vec{J_\epsilon} = -\vec{E} \cdot \vec{J_e} - \Theta_e \tag{1}$$

$$\vec{J_{\epsilon}} = -\mu_{\epsilon} n_{e} \vec{\epsilon_{e}} \vec{E} - D_{\epsilon} \vec{\nabla} (n_{e} \vec{\epsilon_{e}}) \tag{2}$$

where n_e is the electron number density, t the time, $\vec{J_e}$ and $\vec{J_e}$ the electron energy flux and the electron flux vector, respectively, \vec{E} the electric field vector, Θ_e the power loss in collisions due to elastic, inelastic, ionization and attachment process, and μ_e and D_e the mobility and the diffusion coefficient of mean electron energy, respectively.

In this work, plasma discharge is assumed to be uniform in the parallel direction of electrodes. Therefore, the calculation can be simplified as a one-dimensional problem in the discharge gap, as shown in figure 2. The same geometry of dielectric layer thickness of 1.59 mm and gap distance of 14 mm with experiment is used in the numerical modeling. The experimentally measured voltage waveform is applied to the electrodes. The mesh size is $10\,\mu\text{m}$. The initial electron density and accumulated surface charge are considered as adjusted parameters to fit the experiment measurements. The ion density is given by quasi-neutrality. The time step is determined by the shortest characteristic timescale of the drift dynamics

of charged species, plasma kinetics and fluid dynamics for all grids. Point A in figure 2 indicates the central position of discharge gap which is used to compare with experimental measurements.

A modified CH₄/Ar plasma kinetic model from [57, 58] is used in this work, which can be found in supplementary materials. The chemical reactions between ground states are not considered due to the nanosecond timescale studied in this work. The plasma kinetic model consists of 16 species and 48 reactions. Neutral species Ar, CH₄, CH₃, CH₂, CH, C, H₂, H; electronically excited species Ar*, Ar₂; ions Ar⁺, Ar₂⁺, CH₄⁺, CH₃⁺, CH₂⁺; and electrons are included in the model. The vibrationally excited $CH_4(\nu_{2,4})$ bending modes and $CH_4(\nu_{1,3})$ stretching modes are considered to provide gas heating by vibrational–translational relaxation reactions [59]. The rate constants of electron impact reactions, the transport parameter for electrons, and power loss in collisions are pre-calculated by using BOLSIG+ [60]. The cross-sections of electron impact reactions are obtained from the online database LXCat [61]. The cross-sections of Ar are obtained from the Phelps database [62] and B-spline R-matrix (BSR) database [63, 64]. The vibrational cross-sections of CH₄ are obtained from the IST-Lisbon database [65]. The cross-section data of electron impact CH₄ dissociation reactions are calculated from Janev and Reiter's methods [66]. The CH₄ ionization cross-sections are obtained from Straub et al [67].

3. Results and discussion

3.1. Time-resolved measurements of coupling between electron properties and the electric field

First, to investigate the sensitivity of the plasma properties to CH₄ mole fraction, Thomson scattering measurements were conducted at a fixed time delay of 80 ns relative to the start of the nanosecond pulse at varying CH₄ mole fractions in Ar dilution. As shown in figure 4, there is a nonlinear decrease in the electron density as the CH₄ percentage of the mixture increases. We have previously studied such a decrease in electron density with He dilution in ns-DBD [9, 13]. From the model predictions, it was shown that the addition of CH₄ significantly modifies the breakdown process, resulting in decreases of the peak reduced electric field even with 1% CH₄ addition. Here, we see the same behavior where there was a 40% difference between 0% CH₄ and 1% CH₄ and a 15% difference between 1% and 3% CH₄. Unlike the He case, the CH₄ percentage can be increased up to 8% until the instrument detection limit is reached. At this stage, the electron number density starts to plateau. Beyond this point, it was difficult to reliably sustain the plasma with the continuous 8.5 kV pulse train at 500 Hz.

In figure 5, the time-resolved electron number densities, electron temperatures, and electric fields for 0%, 1%, and 5% CH₄ addition are plotted. A reduced electric field axis calculated from a gas temperature of 293 K is provided for reference. In the time-resolved data, the pure Ar trace again had the highest electron number density followed by 1% and 5% CH₄ addition. However, the shape of the temporal profiles of

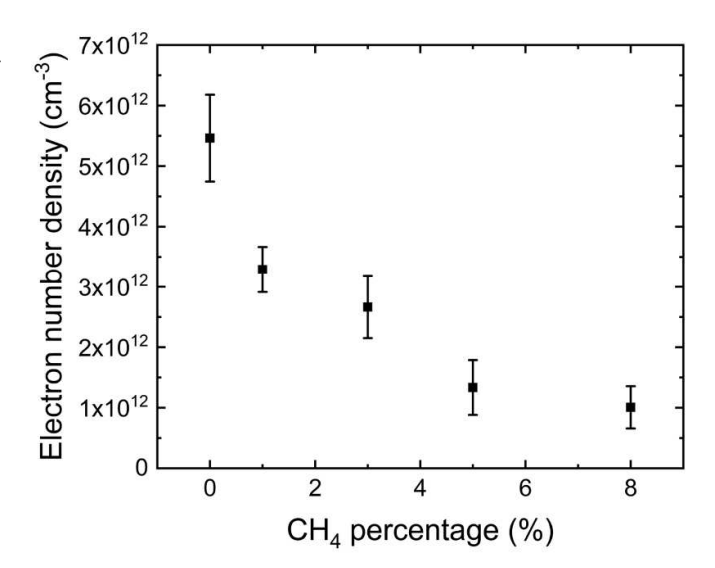


Figure 4. Measured electron number densities as a function of CH_4 mole fraction in an Ar ns-DBD. The 95% confidence intervals of the fit was used as the error bars.

the pure Ar discharge and discharges with CH₄ were markedly different. The pure Ar electron number density increased in the early stage of the discharge and did not decay during the later stage in the discharge. However, for CH₄ containing mixtures, this trend was reversed and the electron density was on a decreasing trend. This could be due to the availability of additional electron energy transfer pathways in CH₄ into vibrations and dissociative electronic excitations. This would then remove energy available for ionization as well as metastable Ar* necessary for step-wise ionization.

Contrary to what was observed in He [9, 13], the electron temperature increased with CH₄ addition. On one hand, holding deposited energy constant, one might expect increasing electron temperatures with decreasing electron number density based on conservation of energy. On the other hand, CH₄, as discussed previously, introduces additional pathways for electron energy loss, particularly at low reduced electric fields. It was on this basis that the decreasing electron temperature trends with increasing CH₄ mole fraction were explained in [9, 13]. This raises the question of why the electron temperature during the voltage sub-pulses increased with CH₄ addition.

To investigate this question further, we employed EFISH to measure the electric fields for these three mixtures. From figure 5, the peak electric fields *increase* with higher CH₄ mole fraction. Shortly after breakdown, the sheath forms and the measured electric field decreases. Even after breakdown, there are corresponding electric field peaks along the rising and falling edges of the applied voltage. Note that EFISH as implemented in this work only gives the magnitude of the electric field strength. In [13], such oscillations in electric field were predicted in a CH₄/He ns-DBD by the model, but unfortunately electric field measurements were unavailable.

Considering all three plasma properties together, the overall picture can be explained as follows. First, the consumption of energy by modes of CH₄ during the rising edge of the voltage pulse reduces the ionization rate and delays breakdown.

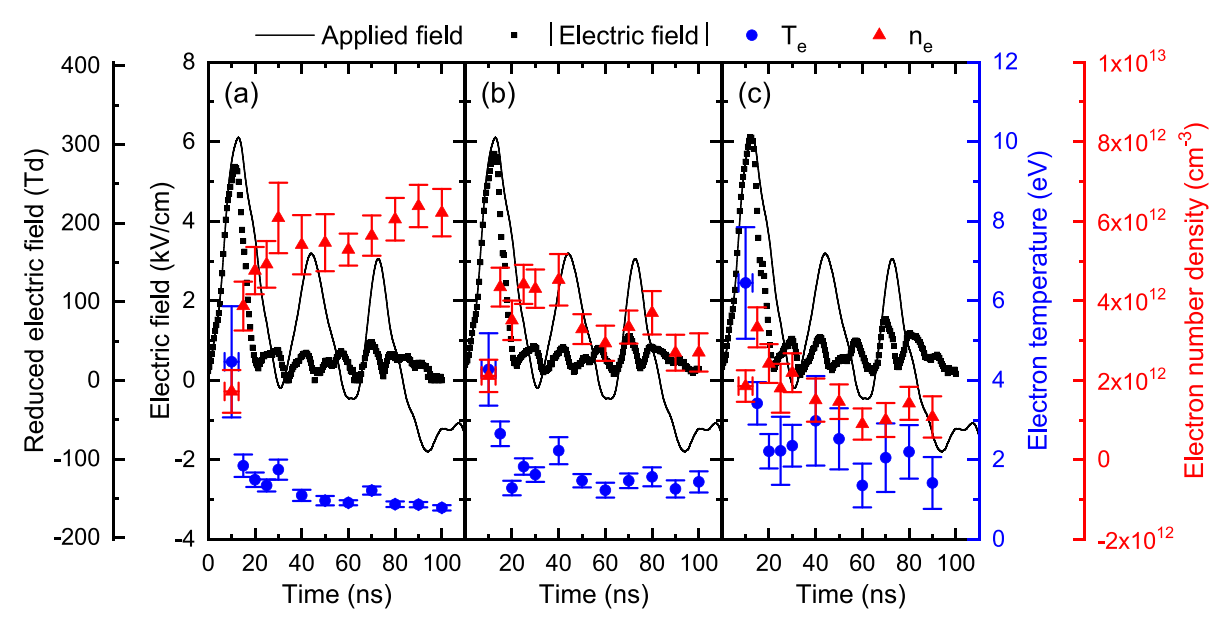


Figure 5. Time-resolved absolute electric field magnitudes, electron temperatures, and electron densities for 0% CH₄ (a), 1% CH₄ (b), and 5% CH₄ (c) mixtures diluted with Ar. All sub-plot x and y-axis scales are identical. Error bars shown represent 95% confidence intervals of the fits.

For example, vibrational excitation of CH₄ and dissociation of CH₄ have threshold energies of 0.16 eV and 9 eV, respectively [64, 65]. Both of these processes have lower threshold energies than excitation to the lowest electronically excited state of Ar, which has a threshold energy of 11.55 eV [64]. Therefore, the peak electric field increases with higher CH₄ mole fraction but the electron number density decreases. As the voltage falls around 20 ns, the electric field decreases and the applied voltage even becomes slightly negative. At this point, electrons just outside the cathode sheath or accumulated on the anode dielectric surface are accelerated toward the cathode and away from the anode, respectively. The sheath collapses and the cathode and anode switch places briefly. The sheath reforms once the next sub-pulse arrives and the cycle continues while the voltage continues varying. This type of field oscillation was also observed in the atmospheric pressure ns-DBD in [68, 69]. From the analytical expressions for a ns-DBD in [70], the electric field in the plasma is inversely proportional to electron number density. Physically, higher charge density results in faster shielding of rapid changes in electric field. With reduced electron number density from CH₄ addition, the electric field oscillations increase in magnitude during the subpulses. An increase in electric field strength heats the electrons and results in higher electron temperature. Therefore, raising the CH₄ mole fraction increases the electron temperature.

This effect is not as strong in He, likely because excitation to electronic states of He have threshold energies above 19.8 eV. Therefore, CH₄ addition is expected to decrease the electron energy more in He than in Ar. This is confirmed in figure 6, where BOLSIG+ calculations were run for different mixtures of CH₄ in He and Ar. For the same reduced electric field, the mean electron energy changes significantly for He mixtures but does not for Ar mixtures. As a result, the electron temperature in He will change for varied CH₄ concentrations.

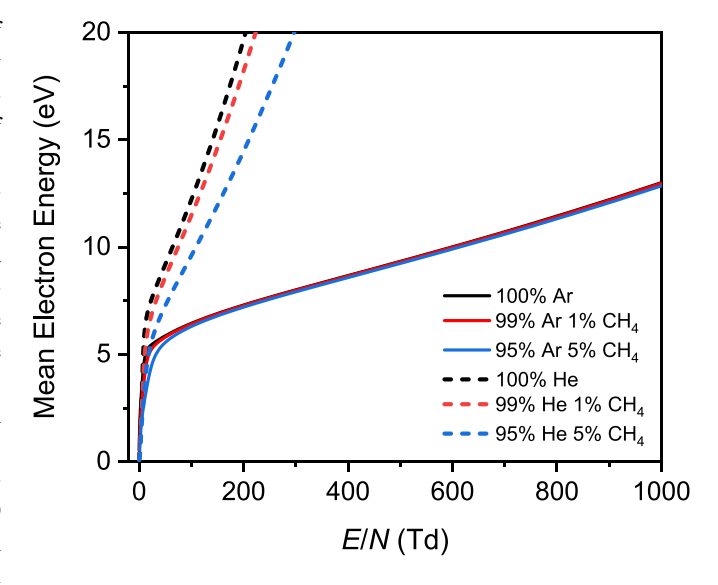
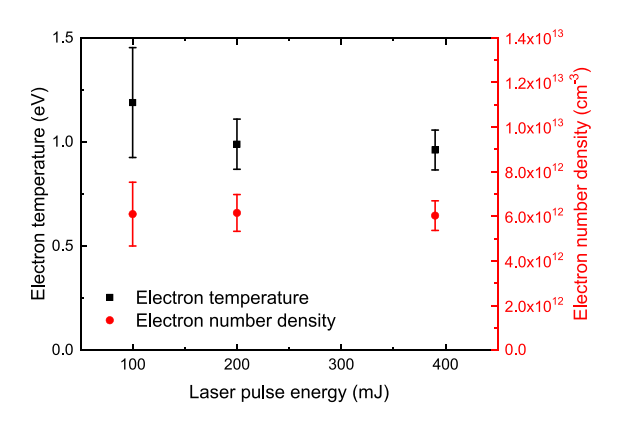


Figure 6. Calculated mean electron energies as a function of reduced electric field for pure Ar, 1% CH₄/Ar, 5% CH₄/Ar, pure He, 1% CH₄/He, and 5% CH₄/He gas mixtures.

In contrast, the electron temperature in Ar will be dominated by electric field heating via the mechanism discussed earlier to explain figure 5.

Much like the hybrid ns/RF discharge in [71], the sub-pulses are fast varying voltage waveforms that drive low E/N excitation. While [71] measured the parameters enhanced by low E/N excitation such as rotational-vibrational non-equilibrium, the electron properties themselves were not measured. Here, we have experimentally identified a direct connection between sub-breakdown electric fields, electron density, and electron heating in ns-DBD plasmas. Similar low E/N excitation can be achieved by pairing ns pulses



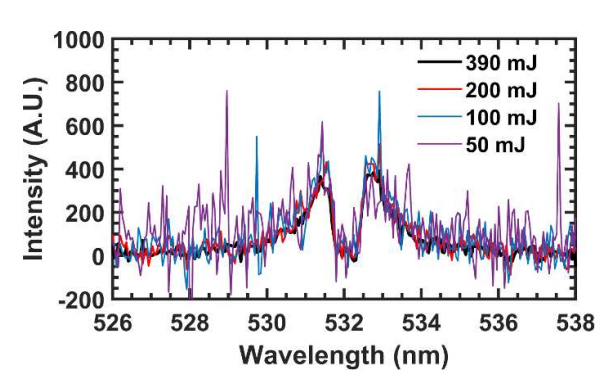


Figure 7. Measured electron temperature and densities 150 ns after the voltage pulse for various laser pulse energies (left). Raw data normalized by the pulse energy is shown (right). Error bars denote fitting uncertainty.

with AC voltages [72, 73], DC voltages [73], and ms tails [27], but only the electric fields have been measured in these discharges.

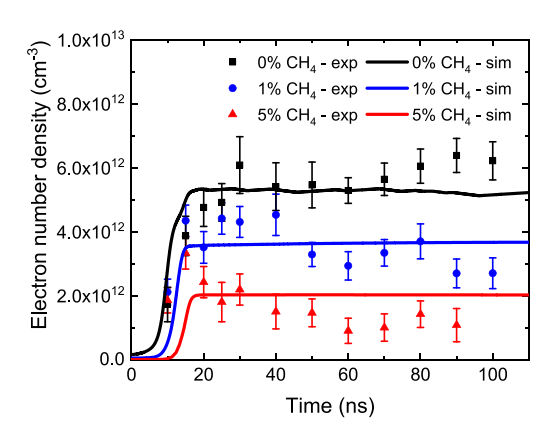
Since these measurements will be compared to numerical simulations, it is important to consider sources of measurement error. It is well-known that Thomson scattering can perturb the plasma if the laser intensity is too high [18, 43]. The most straightforward check is to vary the laser pulse energy and see if the evaluated electron properties change. The results of a laser energy scan from 100 mJ to 390 mJ in pure Ar at a time delay of 150 ns is plotted in figure 7. A 50 mJ spectrum is shown in figure 7, but the signal-to-noise ratio was insufficient for reliable fitting. It can be seen that all of the points lie within the fitting error. Ponderomotive forces can also perturb the measured electron density, but the measured electron densities are orders of magnitude higher than the 10¹⁰ cm⁻³ threshold suggested by [74] to consider such effects. Under current experimental conditions, the perturbation is on the order of 0.01% to the electron density. The detection limit was estimated from figure 7 as 3.8×10^{11} cm⁻³ at a signal-to-noise ratio of 1. The EFISH measurements are calibrated separately prior to the plasma experiments, so evaluation of the calibration is necessary. In figure 5, prior to breakdown, the EFISH measurements closely match the ns pulse waveform to within several hundred V cm⁻¹. Therefore, it is unlikely that there are any substantial errors in the calibration itself. Recently, it has been shown that Gouy phase shift effects can significantly influence the EFISH signal in non-uniform electric fields [31, 75]. In [31], it was found that the EFISH diagnostic performed poorly when the electric field was double peaked during the passage of the narrow fast ionization wave. For electric fields that had a peak centered at the beam focus, the EFISH accuracy using an optimal Rayleigh length was $\pm 10\%$. In diffuse ionization waves, EFISH measurements have compared well with numerical modeling [33, 52]. This suggests that in diffuse discharges the Laplacian electric field profiles are not substantially different from that in the plasma and do not significantly impact the EFISH accuracy. We have previously imaged a similar CH₄/Ar ns-DBD plasma with 1 ns time steps and showed it was diffuse [34]. However, time-resolved ICCD imaging has not been performed in this exact discharge, so it is possible that there are non-uniformities and phase-shift effects that are not accounted for here.

3.2. Experimental validation of a 1D plasma fluid model

Next, we use the experimentally measured plasma properties to evaluate the predictions of a 1D plasma fluid model. As mentioned before, this model is based on the PASSKEy code previously used in surface ns-DBD discharges at atmospheric pressure. However, the electron Boltzmann equation was solved in the quasi-stationary approach, which may not be valid due to reduced electron-neutral collision frequency [76]. Therefore, the present experimental data provides an opportunity to evaluate the model's predictions and investigate the senstivities of the model to surface charge accumulation and the electron-impact cross-sections.

Plotted in figure 8 are the comparisons between the experimental and simulated electron properties. Additionally, the model was able to capture the qualitative trends in the electron densities. However, the electron densities at the rising edge (0-20 ns) did not agree as well with the experiment for the mixtures containing CH₄. This may be due to fast electronion recombination from hydrocarbon cluster ions [77], which were not included in the present kinetic mechanism. Nonetheless, the overall agreement with the experiment was good. For the electron temperature, the peak electron temperatures were well-predicted, but only the 5% CH₄ mixture agreed with the experiment in the late stages of the discharge. For mixtures with lower CH₄ concentrations (higher Ar dilution), the electron temperatures showed the opposite trend to the experimental measurements and increase with lower CH4 mole fraction. Since the source of the electron energy is the electric field, the measurements and predictions of the electric field are plotted in figure 9. A reduced electric field axis calculated using a gas temperature of 293 K is plotted for reference.

In figure 9, the overall trends were predicted by the model. In both the peak electric field and the sub-pulses, higher CH₄ mole fraction led to larger electric fields, and quantitative agreement within half a percent was achieved in the peak electric fields (calculated by the difference in the maximums of the experiment and model). However, the electric field strengths



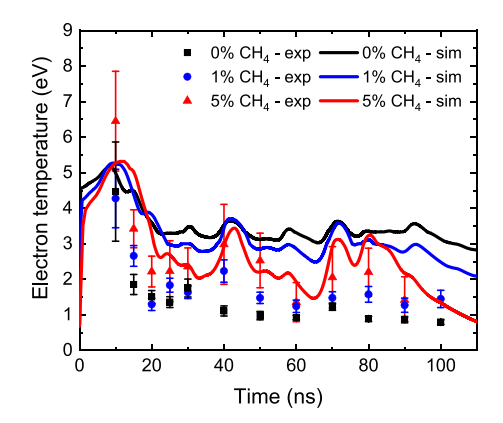


Figure 8. Experimental and simulated electron properties for 0% CH₄, 1% CH₄, and 5% CH₄ mixtures diluted with Ar. The BSR Ar electron-impact cross-sections were used.

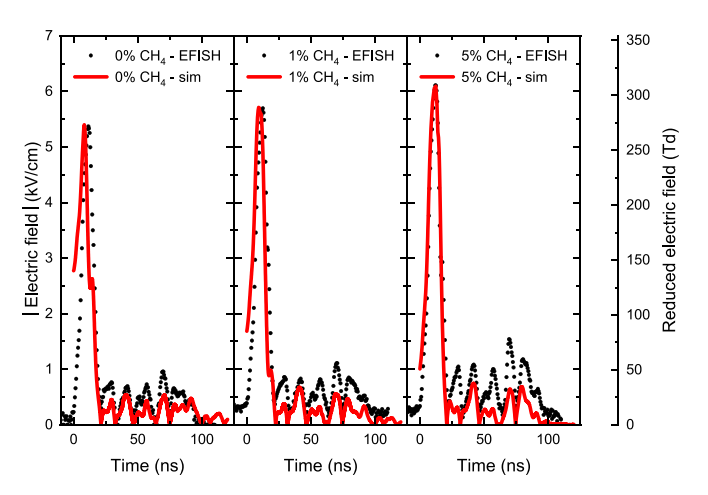


Figure 9. Experimental (absolute) and simulated electric fields for 0% CH₄, 1% CH₄, and 5% CH₄ mixtures diluted with Ar. The BSR Ar electron-impact cross-sections were used.

during the sub-pulses were under-predicted by up to a factor of three. The starting electric field strength at 0 ns for each of the cases was non-zero, since the surface charge accumulation left on the dielectric surfaces between the pulses was unknown. As we will show later, the electric field profiles are sensitive to the amount of surface charge accumulation assumed in the model. Nevertheless, the electric field predictions demonstrate that the source of the opposite trend in electron temperature is not the electric field. In fact, the modeled electric fields increase with larger CH₄ mole fraction which implies that the electron temperatures should also increase. To investigate this further, we examined the electron-impact cross-sections more closely.

3.3. Effects of choice of Ar electron-impact cross-sections

Due to the worse electron energy predictions for low CH_4 concentrations (high Ar dilution), we compared the Ar electron-impact cross-sections from the databases available in LXCat. In the above simulations, we used the BSR database for the Ar cross-sections [63]. These are the most recently updated theoretical cross-sections which were calculated *ab initio*. As shown in figure 10, the electron energies calculated by the BSR

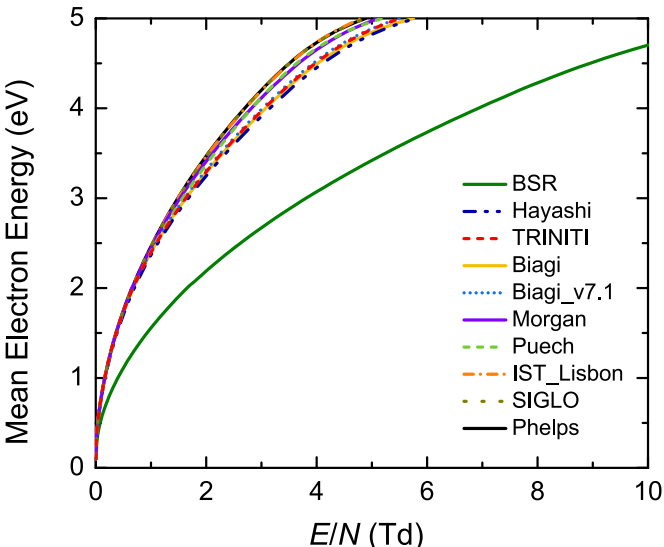
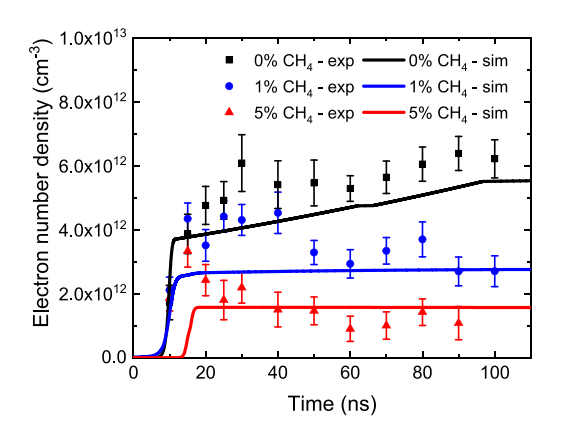


Figure 10. Comparison of mean electron energies calculated by BOLSIG+ for the Ar electron-impact cross-section databases available on LXCat as a function of reduced electric field.

cross-sections are significantly lower than the other databases at low reduced electric fields. In the analysis of the Ar crosssections available in the LXCat database in [78], they noted that the BSR database cross-sections for some processes were significantly different from experimentally measured ones. However, they found that the BSR cross-sections performed well in predicting the electron swarm parameters. In [63], it was claimed that some experimental measurements may have been inaccurately normalized, which lead to higher experimental uncertainty and the observed discrepancies. Even for the BSR cross-sections, the mean electron energy at low E/N (<5 Td) can be more than 3 eV, which explains the elevated electron temperatures predicted in figure 8. Since adding CH₄ introduces energy loss pathways at low E/N due to vibrational excitation, the predicted electron temperature decreased in the model.

However, it is still unclear how the differences in Ar electron-impact cross-sections will impact the simulated plasma properties. To understand the sensitivity of the model



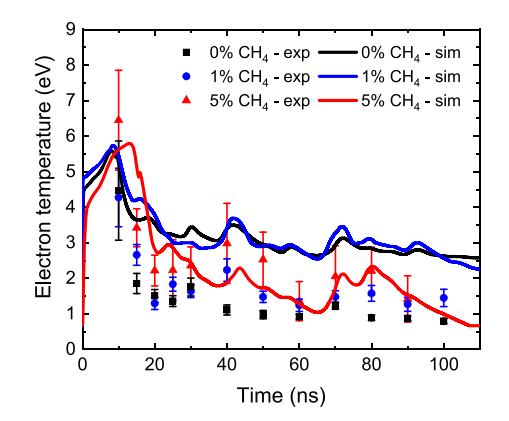


Figure 11. Experimental and simulated electron properties for 0% CH₄, 1% CH₄, and 5% CH₄ mixtures diluted with Ar. The Phelps Ar electron-impact cross-sections were used.

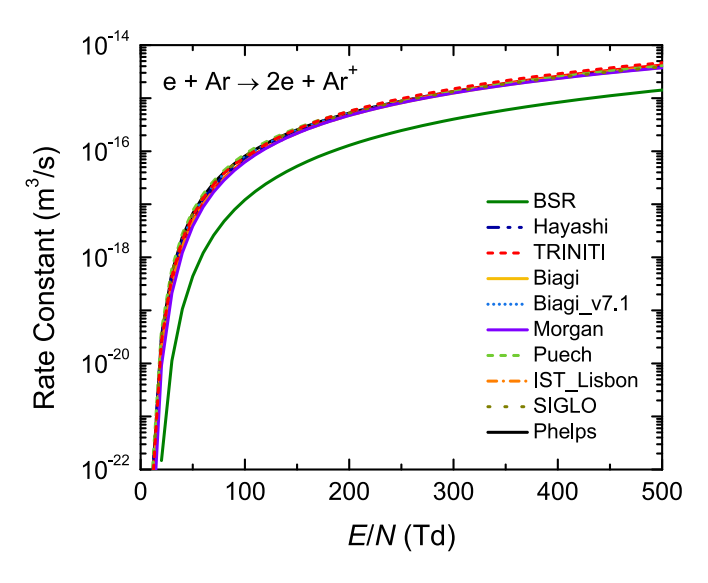


Figure 12. Comparison of ionization rate constants calculated for the Ar electron-impact cross-section databases available on LXCat as a function of reduced electric field.

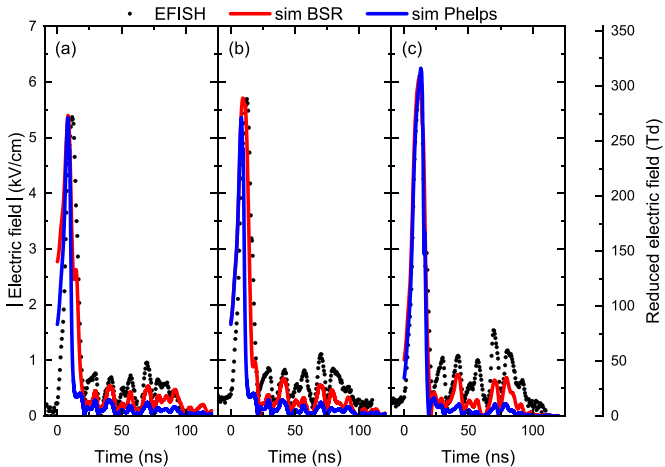


Figure 13. Experimental (absolute) and simulated electric fields for 0% CH₄ (a), 1% CH₄ (b), and 5% CH₄ (c) mixtures diluted with Ar. Simulations using the Phelps cross-sections and the BSR cross-sections are shown.

to the choice of cross-sections, we ran the simulations with the Phelps database cross-sections. The Phelps database is widely used for modeling nanosecond-pulsed discharges containing Ar [57, 79–82], which makes it especially important to compare against the BSR cross-sections.

The electron densities and temperatures for the three CH₄/Ar mixtures are plotted in figure 11. The predictions for the electron temperature were similar to that of figure 8, but a direct trend cannot be established from figure 11. The peak electric fields still increase with higher CH₄ mole fraction, but the sub-pulse electric fields for the 1% CH₄ mixture were larger than those in pure Ar. The gap between the experiment and the modeling predictions of the 5% CH₄ sub-pulse electric fields were also larger with the Phelps cross-sections.

Interestingly, the electron number density for the pure Ar case steadily increased throughout the voltage pulse train. To understand why, the rate constants for the ionization of neutral Ar are plotted in figure 12. The rate constant calculated using the BSR is lower than the Phelps and other databases by an

order of magnitude or more for reduced electric fields below 100 Td. Therefore, the simulations using the Phelps database predicts ionization of Ar, even during the sub-pulses where the reduced electric field is low (<40 Td). Once the sub-pulses end, the electron density profile becomes flat, even though the electron temperature is still predicted to be around 3 eV. This indicates that it is due to the larger ionization cross-section of Ar for the Phelps database that drives this increasing trend in electron number density.

The predicted electric fields calculated with the Phelps and BSR database cross-sections are plotted with the measured electric fields in figure 13. The peak electric fields are well-predicted, but the time of breakdown as well as the sub-pulse electric field magnitudes were not well predicted. The plasma breaks down much earlier than what was observed in the measurements for the 0% and 1% CH₄ mixtures. The electric field oscillations from the sub-pulses were smaller than those calculated by the BSR database by approximately a factor of two. Overall, the BSR gives better predictions for all of the plasma properties, except for the electron number density in pure Ar.

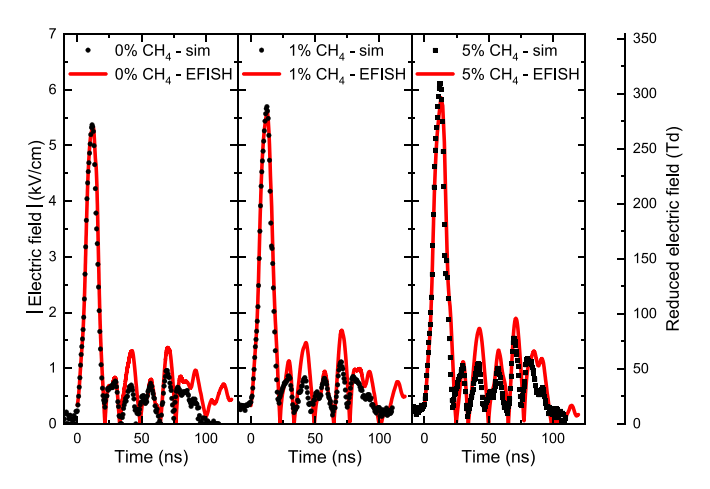


Figure 14. Experimental (absolute) and simulated electric fields for 0% CH₄, 1% CH₄, and 5% CH₄ mixtures diluted with Ar. The BSR Ar electron-impact cross-sections were used. Surface charge was not considered in these simulations.

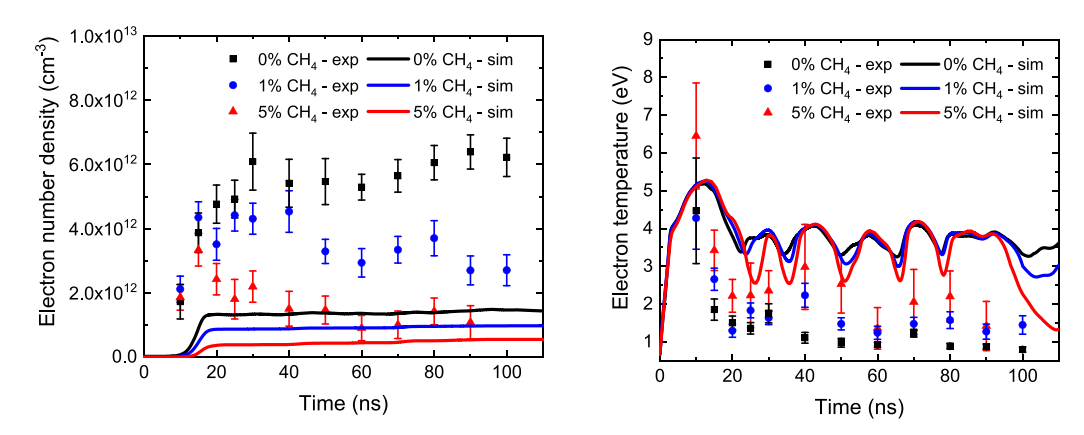


Figure 15. Experimental and simulated electron properties for 0% CH₄, 1% CH₄, and 5% CH₄ mixtures diluted with Ar. The BSR Ar electron-impact cross-sections were used.

However, the poor prediction of electron temperatures at low E/N for the 0% and 1% CH₄ mixtures has not been resolved. It could be that impurities in the Ar gas cylinder play a role in the electron kinetics, or there are significant uncertainties in the electron calculation at low E/N by using the present Ar electron-impact cross-sections even with the BSR database. More measurements and simulations are necessary to clarify this point.

3.4. Impact of surface charge accumulation on predicted plasma properties

During the experiments, the ns-DBD was left free-running at 500 Hz, so the surface charge accumulation between pulses could play a role in the discharge dynamics. As mentioned previously, the above simulations varied the amount of surface charge accumulation on the quartz. Here, we present simulations and their comparisons to the experiment without considering surface charge accumulation, i.e. setting the net surface charge to zero.

In figure 14, the experimentally measured and simulated electric fields are plotted. The simulated electric fields show good agreement with the experimentally measured ones. Both the electric field magnitude and trends with gas mixture

composition were better predicted than in figure 9. However, as shown in figure 15, both the electron number densities and temperatures were not predicted well. The electron number densities were underpredicted by more than a factor of three, and the predicted electron temperatures were larger than the measurements for all mixtures. This demonstrates that the ns-DBD is highly sensitive to the assumed surface charge accumulation. Furthermore, and perhaps more importantly, matching simulated and experimental electric field profiles does not guarantee that the electron properties will be predicted correctly. This highlights the urgent need for more experiments where electric field, electron temperature, and electron density are measured in the same plasma.

4. Conclusions

In this study, we used time-resolved *in situ* laser diagnostics and numerical modeling to investigate the coupling between the reactant composition and plasma properties in CH₄/Ar ns-DBD discharges. Both laser Thomson scattering and EFISH were used to quantify the electron properties and electric field strength, respectively. By changing the CH₄ mole fraction, the electron temperature and electron density

changed non-linearly. While the electron density decreased with increasing CH₄ concentration, the electron temperature increased due to corresponding increases in the electric field. Both the peak electric field as well as oscillations due to subpulses from the voltage power supply increased with CH₄ concentration. We argued that the decrease in electron density led to less efficient shielding of rapid fluctuations in applied electric field, thereby allowing larger electric field strengths to penetrate into the plasma. These larger electric fields heated the electrons and led to the observed increase in electron temperature. Therefore, in this work we have observed a direct non-linear coupling between the plasma properties and reactant mixture composition through the combined usage of laser Thomson scattering and EFISH.

The predictions of the numerical model were evaluated with the experimental measurements, and key areas of uncertainty were revealed. First, better agreement between the experiment and simulation was obtained with higher CH₄ concentration. This indicated that there was uncertainty associated with the Ar electron-impact cross-sections. Simulations using the ab initio calculated cross-sections from the BSR database predicted the plasma properties better than the simulations using the Phelps cross-sections. However, a large discrepancy in the electron temperature remained, even with the BSR cross-sections. Second, we identified the residual dielectric surface charge as a key variable for predicting the plasma properties. When the surface charge was set to zero in the simulation, we found severe under-prediction of the electron density and over prediction of electron temperature. However, the electric field profiles compared well with the experiment. This highlights the need for more multi-parameter measurements of electron density, electron temperature, and electric field in the same discharge as well as comparison with numerical models. Only with measurements of all of these plasma properties can numerical models be fully validated.

In view of these conclusions and the increasing prevalence of laser Thomson scattering, EFISH, and other *in situ* diagnostics of plasma properties in the literature, the combination of these diagnostics for multi-parameter probing of non-equilibrium plasmas should be a key priority for the community moving forward. Comparison of measured and simulated electron properties *and* electric fields will be vital for further development of plasma kinetic models and optimization of plasmas for applications such as CH₄ reforming, catalysis, materials synthesis, medicine, and combustion.

Data availability statement

The data that support the findings of this study are available upon reasonable request from the authors.

Acknowledgment

This work was supported by ExxonMobil through its membership in the Princeton E-filliates Partnership of the Andlinger Center for Energy and the Environment. T Y Chen was

partially supported through the Program in Plasma Science and Technology at Princeton University Fellowship. Y Ju would like to thank the funding support of NETL UCFER, NSF Grants CBET 1903362 and NSF EFRI DCheM-2029425, DOE grant of DE-SC0021217, and DOE Grant DE-SC0020233 of Plasma Science Center.

ORCID iDs

Timothy Y Chen https://orcid.org/0000-0003-3026-9767 Hongtao Zhong https://orcid.org/0000-0003-4064-6298 Benjamin M Goldberg https://orcid.org/0000-0002-1595-0450

References

- [1] Saunois M, Jackson R B, Bousquet P, Poulter B and Canadell J G 2016 The growing role of methane in anthropogenic climate change *Environ. Res. Lett.* 11 120207
- [2] Ocko I B, Sun T, Shindell D, Oppenheimer M, Hristov A N, Pacala S W, Mauzerall D L, Xu Y and Hamburg S P 2021 Acting rapidly to deploy readily available methane mitigation measures by sector can immediately slow global warming *Environ. Res. Lett.* 16 054042
- [3] Scapinello M, Delikonstantis E and Stefanidis G D 2017 The panorama of plasma-assisted non-oxidative methane reforming *Chem. Eng. Process.: Process Intensif.* 117 120–40
- [4] Bogaerts A, De Bie C, Snoeckx R and Kozák T 2017 Plasma based CO₂ and CH₄ conversion: a modeling perspective Plasma Process. Polym. 14 1600070
- [5] Bogaerts A et al 2020 The 2020 plasma catalysis roadmap J. Phys. D: Appl. Phys. 53 443001
- [6] Tao X, Bai M, Li X, Long H, Shang S, Yin Y and Dai X 2011 CH₄–CO₂ reforming by plasma–challenges and opportunities *Prog. Energy Combust. Sci.* 37 113–24
- [7] Khalifeh O, Mosallanejad A, Taghvaei H, Rahimpour M R and Shariati A 2016 Decomposition of methane to hydrogen using nanosecond pulsed plasma reactor with different active volumes, voltages and frequencies *Appl. Energy* 169 585–96
- [8] Wang X, Gao Y, Zhang S, Sun H, Li J and Shao T 2019 Nanosecond pulsed plasma assisted dry reforming of CH₄: the effect of plasma operating parameters *Appl. Energy* 243 132–44
- [9] Chen T Y, Rousso A C, Wu S, Goldberg B M, van der Meiden H, Ju Y and Kolemen E 2019 Time-resolved characterization of plasma properties in a CH₄/He nanosecond-pulsed dielectric barrier discharge *J. Phys. D:* Appl. Phys. 52 18LT02
- [10] Van de Steeg A W, Butterworth T, Van den Bekerom D C M, Silva A F, Van de Sanden M C M and Van Rooij G J 2020 Plasma activation of N₂, CH₄ and CO₂: an assessment of the vibrational non-equilibrium time window *Plasma* Sources Sci. Technol. 29 115001
- [11] Huang B, Zhang C, Bai H, Zhang S, Ostrikov K and Shao T 2020 Energy pooling mechanism for catalyst-free methane activation in nanosecond pulsed non-thermal plasmas *Chem. Eng. J.* 396 125185
- [12] Butterworth T, van de Steeg A, van den Bekerom D, Minea T, Righart T, Ong Q and van Rooij G 2020 Plasma induced vibrational excitation of CH₄-a window to its mode selective processing *Plasma Sources Sci. Technol.* 29 095007

- [13] Chen T Y, Taneja T S, Rousso A C, Yang S, Kolemen E and Ju Y 2021 Time-resolved in situ measurements and predictions of plasma-assisted methane reforming in a nanosecond-pulsed discharge Proc. Combust. Inst. 38 6533-40
- [14] Van de Sande M J 2002 Laser Scattering on Low Temperature Plasmas (Eindhoven: Eindhoven University of Technology)
- [15] Barnat E V and Frederickson K 2010 Two-dimensional mapping of electron densities and temperatures using laser-collisional induced fluorescence *Plasma Sources Sci. Technol.* 19 055015
- [16] van der Meiden H J 2011 Thomson scattering on low and high temperature plasmas *PhD Thesis* Technische Universiteit Eindhoven, Eindhoven, The Netherlands
- [17] Roettgen A, Shkurenkov I, Simeni Simeni M, Petrishchev V, Adamovich I V and Lempert W R 2016 Time-resolved electron density and electron temperature measurements in nanosecond pulse discharges in helium *Plasma Sources Sci. Technol.* 25 055009
- [18] Schregel C, Carbone E A D, Luggenhölscher D and Czarnetzki U 2016 Ignition and afterglow dynamics of a high pressure nanosecond pulsed helium micro-discharge: I. Electron, Rydberg molecules and He (2³S) densities *Plasma* Sources Sci. Technol. 25 054003
- [19] Miles J, Murray C, Ross A, Lemmer K, Russell J and Adams S 2020 Time resolved electron density and temperature measurements via Thomson scattering in an atmospheric nanosecond pulsed discharge *Plasma Sources Sci. Technol.* 29 07LT02
- [20] Yong T, Abdalla A I and Cappelli M A 2021 Laser absorption measurements of electron density in nanosecond-scale atmospheric pressure pulsed plasmas *Phys. Plasmas* 28 053501
- [21] Ito T, Kobayashi K, Czarnetzki U and Hamaguchi S 2010 Rapid formation of electric field profiles in repetitively pulsed high-voltage high-pressure nanosecond discharges J. Phys. D: Appl. Phys. 43 062001
- [22] Goldberg B M, Shkurenkov I, O'Byrne S, Adamovich I V and Lempert W R 2015 Electric field measurements in a dielectric barrier nanosecond pulse discharge with sub-nanosecond time resolution *Plasma Sources Sci. Technol.* 24 035010
- [23] Dogariu A, Goldberg B M, O'Byrne S and Miles R B 2017 Species-independent femtosecond localized electric field measurement *Phys. Rev. Appl.* 7 024024
- [24] Goldberg B M, Chng T L, Dogariu A and Miles R B 2018 Electric field measurements in a near atmospheric pressure nanosecond pulse discharge with picosecond electric field induced second harmonic generation Appl. Phys. Lett. 112 064102
- [25] Chng T L, Brisset A, Jeanney P, Starikovskaia S M, Adamovich I V and Tardiveau P 2019 Electric field evolution in a diffuse ionization wave nanosecond pulse discharge in atmospheric pressure air *Plasma Sources Sci. Technol.* 28 09LT02
- [26] Goldberg B M, Reuter S, Dogariu A and Miles R B 2019 1D time evolving electric field profile measurements with sub-ns resolution using the E-FISH method *Opt. Lett.* 44 3853-6
- [27] Tang Y, Simeni M S, Frederickson K, Yao Q and Adamovich I V 2019 Counterflow diffusion flame oscillations induced by ns pulse electric discharge waveforms Combust. Flame 206 239–48
- [28] Butterworth T D and Cha M S 2020 Electric field measurement in electric-field modified flames *Proc. Combust. Inst.* 38 6651–60
- [29] Adamovich I V, Butterworth T, Orriere T, Pai D Z, Lacoste D A and Cha M S 2020 Nanosecond second harmonic generation for electric field measurements with

- temporal resolution shorter than laser pulse duration *J. Phys. D: Appl. Phys.* **53** 145201
- [30] Chng T L, Ding C, Naphade M, Goldberg B M, Adamovich I V and Starikovskaia S M 2020 Characterization of an optical pulse slicer for gas-phase electric field measurements using field-induced second harmonic generation J. Instrum. 15 C03005
- [31] Chng T L, Pai D Z, Guaitella O, Starikovskaia S M and Bourdon A 2022 Effect of the electric field profile on the accuracy of E-FISH measurements in ionization waves *Plasma Sources Sci. Technol.* 31 015010
- [32] Goldberg B M, Hoder T and Brandenburg R 2022 Electric field determination in transient plasmas: in-situ & non-invasive methods Plasma Sources Sci. Technol. 31 073001
- [33] Orr K, Yang X, Gulko I and Adamovich I V 2020 Formation and propagation of ionization waves during ns pulse breakdown in plane-to-plane geometry *Plasma Sources Sci. Technol.* 29 125022
- [34] Rousso A C, Goldberg B M, Chen T Y, Wu S, Dogariu A, Miles R B, Kolemen E and Ju Y 2020 Time and space resolved diagnostics for plasma thermal-chemical instability of fuel oxidation in nanosecond plasma discharges *Plasma Sources Sci. Technol.* 29 105012
- [35] Patel K, Saha A, Zhou T, Meyer T R, Bane S and Satija A 2022 Spectrally filtered ps-ns emission dynamics of atmospheric-pressure nanosecond pulsed plasmas Appl. Phys. Lett. 120 014101
- [36] Simeni M S, Zheng Y, Barnat E V and Bruggeman P J 2021 Townsend to glow discharge transition for a nanosecond pulse plasma in helium: space charge formation and resulting electric field dynamics *Plasma Sources Sci. Technol.* 30 055004
- [37] Paris P, Aints M, Valk F, Plank T, Haljaste A, Kozlov K V and Wagner H-E 2005 Intensity ratio of spectral bands of nitrogen as a measure of electric field strength in plasmas J. Phys. D: Appl. Phys. 38 3894
- [38] Obrusník A, Bílek P, Hoder T, Šimek M and Bonaventura Z 2018 Electric field determination in air plasmas from intensity ratio of nitrogen spectral bands: I. sensitivity analysis and uncertainty quantification of dominant processes *Plasma Sources Sci. Technol.* 27 085013
- [39] Bílek P, Obrusník A, Hoder T, Šimek M and Bonaventura Z 2018 Electric field determination in air plasmas from intensity ratio of nitrogen spectral bands: Ii. reduction of the uncertainty and state-of-the-art model *Plasma Sources Sci. Technol.* 27 085012
- [40] Fiocco G and Thompson E 1963 Thomson scattering of optical radiation from an electron beam *Phys. Rev. Lett.* **10** 89–91
- [41] Gerry E T and Rose D J 1966 Plasma diagnostics by Thomson scattering of a laser beam *J. Appl. Phys.* **37** 2715–24
- [42] van Gessel A F H, Carbone E A D, Bruggeman P J and van der Mullen J J A M 2012 Laser scattering on an atmospheric pressure plasma jet: disentangling Rayleigh, Raman and Thomson scattering *Plasma Sources Sci. Technol.* 21 015003
- [43] Carbone E and Nijdam S 2015 Thomson scattering on non-equilibrium low density plasmas: principles, practice and challenges *Plasma Phys. Control. Fusion* 57 014026
- [44] Roettgen A, Shkurenkov I, Simeni M S, Adamovich I V and Lempert W R 2016 Time-resolved electron temperature and electron density measurements in a nanosecond pulse filament discharge in H₂ -He and O₂ -He mixtures *Plasma* Sources Sci. Technol. 25 055008
- [45] Lefkowitz J K, Guo P, Rousso A and Ju Y 2015 Species and temperature measurements of methane oxidation in a nanosecond repetitively pulsed discharge *Phil. Trans. R.* Soc. A 373 20140333
- [46] Rousso A, Yang S, Lefkowitz J, Sun W and Ju Y 2017 Low temperature oxidation and pyrolysis of n-heptane in

- nanosecond-pulsed plasma discharges *Proc. Combust. Inst.* **36** 4105–12
- [47] Zhong H, Mao X, Rousso A C, Patrick C L, Yan C, Xu W, Chen Q, Wysocki G and Ju Y 2020 Kinetic study of plasma-assisted n-dodecane/O2/N2 pyrolysis and oxidation in a nanosecond-pulsed discharge *Proc. Combust. Inst.* 38 6521–31
- [48] Mao X, Zhong H, Zhang T, Starikovskiy A and Ju Y 2022 Modeling of the effects of non-equilibrium excitation and electrode geometry on H₂/air ignition in a nanosecond plasma discharge *Combust. Flame* 240 112046
- [49] Mao X, Zhong H, Wang Z, Ombrello T and Ju Y 2023 Effects of inter-pulse coupling on nanosecond pulsed high frequency discharge ignition in a flowing mixture *Proc. Combust. Inst.* (https://doi.org/10.1016/j.proci.2022.06.018) accepted
- [50] Zhu Y, Chen X, Wu Y and Starikovskaia S 2021 Passkey code (available at: http://www.plasma-tech.net/parser/passkey/)
- [51] Zhu Y, Shcherbanev S, Baron B and Starikovskaia S 2017 Nanosecond surface dielectric barrier discharge in atmospheric pressure air: I. measurements and 2D modeling of morphology, propagation and hydrodynamic perturbations *Plasma Sources Sci. Technol.* 26 125004
- [52] Zhu Y, Chen X, Wu Y, Hao J, Ma X, Lu P and Tardiveau P 2021 Simulation of ionization-wave discharges: a direct comparison between the fluid model and E-FISH measurements *Plasma Sources Sci. Technol.* 30 075025
- [53] Chen X, Zhu Y, Wu Y, Hao J, Ma X and Lu P 2021 Numerical investigations of nanosecond surface streamers at elevated pressure *Plasma Sources Sci. Technol.* 30 075008
- [54] Chen Z 2009 Studies on the Initiation, Propagation and Extinction of Premixed Flames (Princeton, NJ: Princeton University)
- [55] Chen Z, Burke M P and Ju Y 2009 Effects of Lewis number and ignition energy on the determination of laminar flame speed using propagating spherical flames *Proc. Combust. Inst.* 32 1253–60
- [56] Sun W 2020 Developments of efficient numerical methods for combustion modeling with detailed chemical kinetics *PhD Thesis* Princeton University
- [57] Mao X, Chen Q and Guo C 2019 Methane pyrolysis with N₂/Ar/He diluents in a repetitively-pulsed nanosecond discharge: kinetics development for plasma assisted combustion and fuel reforming *Energy Convers. Manage*. 200 112018
- [58] Mao X, Rousso A, Chen Q and Ju Y 2019 Numerical modeling of ignition enhancement of CH₄/O₂/He mixtures using a hybrid repetitive nanosecond and DC discharge *Proc. Combust. Inst.* 37 5545–52
- [59] Starikovskiy A and Aleksandrov N 2013 Plasma-assisted ignition and combustion *Prog. Energy Combust. Sci.* 39 61–110
- [60] Hagelaar G J M and Pitchford L C 2005 Solving the Boltzmann equation to obtain electron transport coefficients and rate coefficients for fluid models *Plasma Sources Sci. Technol.* 14 722–33
- [61] Pancheshnyi S, Biagi S, Bordage M C, Hagelaar G J M, Morgan W L, Phelps A V and Pitchford L C 2012 The LXCat project: electron scattering cross sections and swarm parameters for low temperature plasma modeling *Chem. Phys.* 398 148–53
- [62] Phelps database (available at: www.lxcat.net) (Accessed 13 August 2021)
- [63] Zatsarinny O, Wang Y and Bartschat K 2014 Electron-impact excitation of argon at intermediate energies *Phys. Rev.* A 89 022706
- [64] Bsr (quantum-mechanical calculations by O Zatsarinny and K Bartschat) (available at: www.lxcat.net) (Accessed 13 August 2021)

- [65] Ist-lisbon database (avilablet at: www.lxcat.net) (Accessed 13 August 2021)
- [66] Janev R K and Reiter D 2002 Collision processes of chy and chy+ hydrocarbons with plasma electrons and protons *Phys. Plasmas* 9 4071–81
- [67] Straub H C, Lin D, Lindsay B G, Smith K A and Stebbings R F 1997 Absolute partial cross sections for electron-impact ionization of CH₄ from threshold to 1000 ev J. Chem. Phys. 106 4430–5
- [68] Ito T, Kanazawa T and Hamaguchi S 2011 Rapid breakdown mechanisms of open air nanosecond dielectric barrier discharges *Phys. Rev. Lett.* 107 065002
- [69] Bak M S and Cappelli M A 2013 Simulations of nanosecond-pulsed dielectric barrier discharges in atmospheric pressure air J. Appl. Phys. 113 113301
- [70] Adamovich I V, Nishihara M, Choi I, Uddi M and Lempert W R 2009 Energy coupling to the plasma in repetitive nanosecond pulse discharges *Phys. Plasmas* 16 113505
- [71] Gulko I, Jans E R, Richards C, Raskar S, Yang X, van den Bekerom D C M and Adamovich I V 2020 Selective generation of excited species in ns pulse/RF hybrid plasmas for plasma chemistry applications *Plasma Sources Sci. Technol.* 29 104002
- [72] Goldberg B M, Shkurenkov I, Adamovich I V and Lempert W R 2016 Electric field in an AC dielectric barrier discharge overlapped with a nanosecond pulse discharge *Plasma Sources Sci. Technol.* 25 045008
- [73] Tang Y, Simeni M S, Yao Q and Adamovich I V 2022 Non-premixed counterflow methane flames in DC/AC/ns electric fields *Combust. Flame* 240 112051
- [74] Shneider M N 2017 Ponderomotive perturbations of low density low-temperature plasma under laser Thomson scattering diagnostics *Phys. Plasmas* 24 100701
- [75] Chng T L, Starikovskaia S M and Schanne-Klein M-C 2020 Electric field measurements in plasmas: how focusing strongly distorts the E-FISH signal *Plasma Sources Sci. Technol.* 29 125002
- [76] Tejero-del Caz A, Guerra V, Pinhão N, Pintassilgo C D and Alves L L 2021 On the quasi-stationary approach to solve the electron Boltzmann equation in pulsed plasmas *Plasma* Sources Sci. Technol. 30 065008
- [77] Anokhin E M, Popov M A, Kochetov I V, Starikovskiy A Y and Aleksandrov N L 2016 Kinetic mechanism of plasma recombination in methane, ethane and propane after high-voltage nanosecond discharge *Plasma Sources Sci. Technol.* 25 044006
- [78] Pitchford L C et al 2013 Comparisons of sets of electron–neutral scattering cross sections and swarm parameters in noble gases: I. Argon J. Phys. D: Appl. Phys. 46 334001
- [79] Aleksandrov N L, Kindysheva S V and Kochetov I V 2014 Kinetics of low-temperature plasmas for plasma-assisted combustion and aerodynamics *Plasma Sources Sci. Technol.* 23 015017
- [80] Yin Z, Eckert Z, Adamovich I V and Lempert W R 2015 Time-resolved radical species and temperature distributions in an Ar–O₂–H₂ mixture excited by a nanosecond pulse discharge *Proc. Combust. Inst.* 35 3455–62
- [81] Luo Y, Lietz A M, Yatom S, Kushner M J and Bruggeman P J 2018 Plasma kinetics in a nanosecond pulsed filamentary discharge sustained in Ar–H₂O and H₂O J. Phys. D: Appl. Phys. 52 044003
- [82] Cheng L, Barleon N, Cuenot B, Vermorel O and Bourdon A 2022 Plasma assisted combustion of methane-air mixtures: validation and reduction *Combust. Flame* 240 111990